Molecular Modelling of Amorphous Kerogen: An Experimental and Theoretical Study

Hyeonseok Lee[2], Farnaz A. Shakib[3*], Kouqi Liu[2], Bo Liu[1], Bailey Bubach[2], Rajender S. Varma[4], Mohammadreza Shokouhimher[2,5*], Mehdi Ostadhassan[1*]

[1]Key Laboratory of Continental Shale Hydrocarbon Accumulation and Efficient Development, Northeast Petroleum University, Daqing 163318, China

[2]Department of Petroleum Engineering, University of North Dakota, Grand Forks, ND 58202, United States

[3]Department of Chemistry and Environmental Science, New Jersey Institute of Technology, Newark, New Jersey 07102, United States

[4]Regional Centre of Advanced Technologies and Materials, Department of Physical Chemistry, Faculty of Science, Palacky University, Šlechtitelů 27, 783 71 Olomouc, Czech Republic

[5]Department of Materials Science and Engineering, Research Institute of Advanced Materials, Seoul National University, Seoul 08826, Republic of Korea

*Corresponding authors' e−mail: mehdi.ostadhassan@nepu.edu.cn, shakib@njit.edu, mrsh2@snu.ac.kr

Abstract

This paper reports the results of grand canonical Monte Carlo (GCMC)/molecular dynamics (MD) simulations of N_2 and CO_2 gas adsorptions on three different organic geomacromolecule (kerogen) models. Molecular models of Kerogen, although being continuously developed through various analytical and theoretical methods, still require further research due to the complexity and variability of the organic matter. In this joint theory and experiment study, three different kerogen models, with varying chemical compositions and structure from the Bakken, were constructed based on the acquired analytic data by by Kelemen et al. in 2007: 13C nuclear magnetic resonance ($^{13}C-NMR$), X−ray photoelectron spectroscopy (XPS), and X−ray absorption near−edge structure (XANES). N_2 and CO_2 gas adsorption isotherms obtained from GCMC/MD simulations are in a very good agreement with the experimental isotherms of physical samples that had a similar geochemical composition and thermal maturity. The N_2/CO_2 uptake by the kerogen model at a range of pressure shows considerable similarity with our experimental data. The stronger interaction of CO_2 molecules with the model leads to the penetration of CO_2 molecules to the sub-surface levels in contrast to N_2 molecules being concentrated on the surface of kerogen. These results suggest the important role of kerogen in the separation and transport of gas in organic rich shale plays that are the target for sequestration of CO_2 and/or enhanced oil recovery (EOR).

Keywords: organic matter; Bakken; macromolecular model; gas adsorption.

Introduction

The worldwide increase of energy consumption was accompanied by a shift of interest from conventional resources to the unconventional shale gas and oil[1] leading to continuous research and development on how to extract from these reservoirs[2,3] even though such reservoirs require more costly and advanced technologies to exploit.[4–6] In these reservoirs, organic matter or kerogen, which is the source of hydrocarbons,[7,8] is a major but poorly understood constituent compared to inorganic minerals. This is mostly because of complexity in chemical composition, structure, and properties of kerogen which originates from its biogenic origin.[9] Kerogen, composed of mainly carbon, hydrogen, oxygen, nitrogen, and sulfur, experiences major structural and compositional changes as it undergoes maturation as a function of burial depth, i.e. pressure and temperature.[10] and finally breaks down to petroleum and other by-products. Maturation is a complex chemical transformation which encompasses free-radical mechanisms, causing the investigating of volumetric, thermodynamic, and stereochemical properties of porous kerogen a highly taxing process. Furthermore, the high submicron porosity of kerogen, drastically impacts the storage and transport properties of the entire shale layer[1,7] and adds another layer of complexity to the investigation of this macromolecule. Therefore, building molecular models for kerogen is a much desired but challenging task, and not surprisingly, it has been continueusly evolving with the advancements in computational methods.[8,11]

The first kerogen model was published by Burlingame et al. in 1968 which had focused on the study of the kerogen extracted from the Green River Shale.[12] The suggested model did not represent a comprehensive chemical structure of the sample though, as it did not contain molecular topology. Later in 1995, Siskin et al. proposed an updated model for kerogen, particularly by adding the functional groups with oxygen and nitrogen.[13] Recent advancements in computational 3D modeling, drastically renewed the interest in exploring kerogen's molecular structure. Varying types of maturity models were introduced for kerogen by Ungerer et al. in 2015[14] wherein they analyzed diverse kerogen types (based on their biogenic origin) grounded on a set of experimental data and PM7 semiemprical calculations as implemented in MOPAC.[15] In addition to the development of the molecular models for this purpose, the computational techniques have also become frequent tools for simulating the gas adsorption and desorption processes.[16–18] Simulation of adsorption behavior is important since organic rich shales are becoming a repository of green

house gases storage which can also improve their productivity in CO_2 enhanced oil recovery (EOR) and sequestration.

The Bakken Formation is one of the largest unconventional shale oil plays in North America and is currently being studied for potential CO_2-enhanced oil recovery and sequestration;[19] recent studies suggest that an injection of CO_2 into organic−rich shales can increase their production potential.[16,19] Hence, in order to precisely estimate the capacity of organic matter in terms of adsorption for sequestration and/or associated mechanisms for enhanced oil recovery, building a 3D molecular model of the Bakken kerogen has become imperative. Here, we report a new representative molecular model for organic matter from the Bakken (kerogen type II) based on previously experimental chemical compositional data.[20] We validate our models with gas (CO_2 and N_2) adsorption isotherms based on both experimental techniques and theoretical simulations. We also investigate CO_2 and N_2 diffusion behavior in kerogen system to present a complete picture of interactions that would occur between kerogen and gas molecules.

Methods

Model Preparation

A variety of methods can be utilized to provide the chemical composition of organic matter. While ^{13}C−NMR is used to examine the chemical structures and parameters related to carbon, the sulfur and nitrogen content are revealed through the X−ray absorption near−edge structure (XANES) analysis. The X−ray photoelectron spectroscopy (XPS) is capable of quantifying several functional groups in carbonaceous materials associated with carbon, oxygen, sulfur, and nitrogen.[21] This information can then be used to build a representative model of any organic material. Here, to build our molecular model of Bakken kerogen, we use the chemical and structural information of kerogen from diverse origins including Bakken, using ^{13}C−NMR, XPS, and XANES data as were reported by Kelemen et al. in 2007.[20] The Bakken organic matter is an immature (pre−oil window) type II kerogen representing a marine environment with T_{max} of 419 °C and hydrogen index (HI) of 580 mg/g.[20] The atomic ratios of carbon, hydrogen, sulfur, and nitrogen atoms were decided by considering the ^{13}C–NMR, XANES, and XPS analysis results. In particular, ^{13}C-NMR data was utilized for carbon and XPS/XANES for heteroatoms estimations to build the molecular model. From this data, around 35% of the total carbon concentation is included within aromatic structures

that also contain nitrogen and sulfur, such as pyridine, pyrrole, and thiophene. The functional groups related to sulfur were set as sulfate and sulfoxide structures, while the oxygen–related functional groups were set as carbonyl and ether.

Throughout the text, the theoretical results obtained from our molecular model of the Bakken kerogen will be compared and contrasted to a set of experimental results from literature[20] plus two other sets of results that were collected from the Bakken (type II) and tested for gas adsorption in our lab. For the ease of comparison, we refer to the first set of experimental results as sample B1 and the other two as samples B2 and B3 (sampled at 8387 and 9814 feet in vetical depths, respectively). The geochemical characteristics of all these three samples, obtained from programmed pyrolysis,[22] are reported in Table 1. It can be seen from this table that the two B2 and B3 samples have the same T_{max} of 429 °C, and hydrogen index (HI) of 555 and 513 mg/g, respectively. Based on this analysis, we conclude that all of these three samples have similar chemical and physical properties and can equivalently represent the immature Bakken kerogen since they are all in the pre-oil generation window. Thus, while we used the data from sample B1 for building molecular models, we obtained the adsorption isotherm data from sample B2 and B3 to verify proposed molecular model.

Table 1. Properties of the Bakken Shale Kerogen Samples, all belonging to type II kerogen and in the pre−oil window (immature).

Property	B1[a]	B2[b]	B3[b]
T_{max}(°C)	419	429	429
HI(mg/g)	580	555	513

[a]Tmax and HI data of Bakken sample B1 were estimated by Kelemen et al.[20]

[b]For Bakken sample B2 and B3, rock-Eval pyrolysis was applied to quantify Tmax and HI.[22]

Molecular Model Building

The construction of macromolecule kerogen models in this paper consists of the following major steps.

a) First, the details of chemical composition including the nature and ratio of functional groups were determined through analyzing the experimental data reported by Kelemen et al.,[20] sample B1.

b) Using this information, fragments of monoaromatic/polyaromatics moieties (benzene, pyrrolic, pyridinic, and thiophene) and functional groups (sulfate, sulfoxide, carboxylate, amino) and alkanes were built using molecular drawing software, Avogadro.[23] These fragments were built using General AMBER Force Field (GAFF) parameters.[24,25] The fragments contained the as accurate number of nitrogen, sulfur, and aromatic carbon atoms as possible based on the experimental data. The partial charges on all atoms were assigned by the Gasteiger−Marsili sigma charges[26] at the initial stage of the macromolecular model building. The nature of bridges (e.g. ketone and ether) between the fragments were assigned based on the sample analysis and were selected to satisfy the number of oxygen, and carbon atoms.

c) In designing aromatic fragments, ^{13}C−NMR data were used to find the percentage of protonated, non−protonated, and bridge carbons, where XPS results were used to obtain the ratio of nitrogen and sulfur−containing aromatic structure.

d) In order to cross−link all of the prebuilt fragments, we used the "bond creation" feature of the LAMMPS package.[27] This feature can create bonds between specified atomic sites as a molecular dynamics (MD) simulation running, if the distance between the two atoms becomes less than a threshold value. As such, we carefully selected the bonding sites in the form of aromatic carbon (protonated, non-protonated) and oxygen-related fragments, because in that format they can better fit the designed model. The pre-built fragments were positioned in a rectangular simulation box using Packmol package.[28] Then, the cross-linkings between the fragments and bridges were generated during an MD trajectory that converged towards local equilibrium with GAFF force field parameters.[25,27] The cross−linked fragment was

e) When the fragments were branched, conforming the desired ratio of hydrogen to carbon atoms led to creation of unpaired free radical sites. Therefore, the cross−linked fragments were inspected and improved maximally by adding or removing hydrogen or methyl groups. Thus, by trial and error process, we built the molecular model of kerogen that interweaves all of the constituent fragments within a single macromolecule.

Quantum Mechanics Calculations

To obtain the quantitative electrostatic properties and optimized geometries of our kerogen model, we performed quantum mechanical (QM) calculations using the ORCA package[29] based on density functional theory (DFT) method. As DFT considered to be suitable for organic compounds, we ran our calculations at B3LYP/6−31G(d) Method/Basis set level.[30] Hirshfeld atomic population[31] analysis was carried out to obtain atomic partial charges since it is less basis−set dependent and can be derived for optimal partitioning of electron density. The partial charges obtained from the QM calculations replaced the initial partial charges which had been set without the polarization of atoms.

Gas Adsorption and Diffusion Simulation (GCMC+MD)

Gas adsorption simulations were carried out using Grand Canonical Monte Carlo (GCMC) simulation, and gas diffusion was utilized by Molecular Dynamics (MD) technique efficiently converging towards local equilibrium for diffusion equation. The equilibrium can be determined in the molecule configuration considering fluctuations in the internal energy and number of adsorbed molecules. We used a hybrid molecular simulation that consists of combining GCMC and MD to perform simulations implemented in LAMMPS package[27,32] (Schematic illustration of the simulation system is shown in Figure 1). At every time step of the simulation, we attempted both GCMC exchanges (insertions and deletions) and MC moves (translations and rotations), followed by MD simulation steps in canonical ensemble at the constant number of molecules. This process allows the gas molecule diffusion and kerogen model relaxation at each GCMC timestep. Technically, every 100 GCMC insertion/deletion attempts followed by 200 MD timesteps. In GCMC simulation, the chemical potential of the gas phase was related to the gas pressure using the ideal gas equation of state. The Metropolis algorithm was utilized to calculate the potential energy in the system and to control GCMC exchange or MC move. The gas adsorption and

diffusion simulations were run for 5×10^7 MD steps and 2.5×10^5 GCMC cycles using a Nose-Hoover thermostat to keep the temperature constant. The time step in all simulations was 1 fs.

Interactions were modeled by the sum of short−range Pauli repulsion and long-range electrostatic attraction embedded within Lennard−Jones potential with a cutoff distance of 10 Å using a particle−particle particle−mesh solver (PPPM).[33,34] The N_2 and CO_2 molecules were simulated using the TraPPE force field parameter sets shown in Table 2,[35] which is useful for complex chemical systems with molecular simulation. In the TraPPE force field, CO_2 was modeled as a linear triatomic and N_2 as a diatomic molecule with fixed bond lengths and bond angles. These models are suitable for reproducing the densities and the diffusion of N_2 and CO_2 in bulk and surface phases at the conditions simulated in this work. The system was set in order to maintain a constant temperature of 77 K and 273 K which is the experimental gas adsorption temperatures and applied with the Nosé−Hoover thermostats. All partial charges of the kerogen models were obtained from QM calculations as explained in the previous section. At equilibrium, the number of gas molecules in the kerogen surface and bulk phase was kept constant.

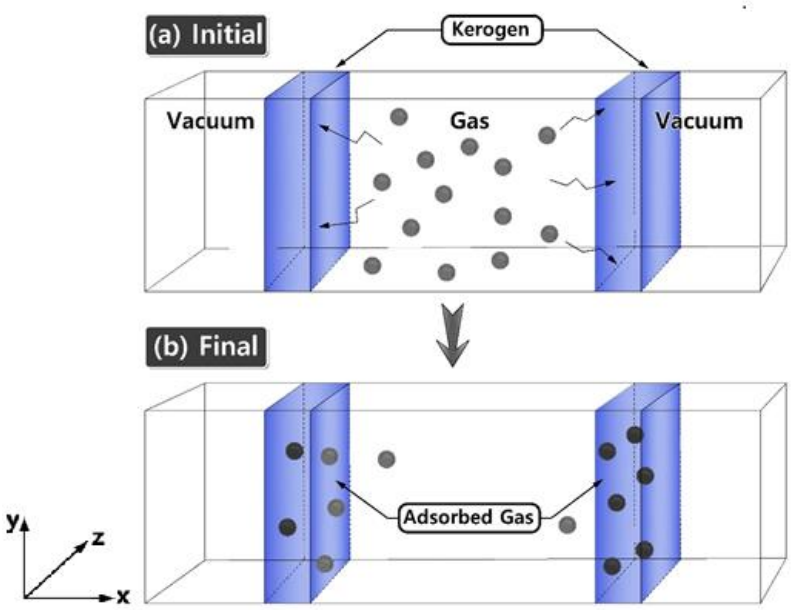

Figure 1. Schematic illustration of the simulation system. (a) Initial gas adsorption/diffusion simulation set-up within the kerogen models. (b) The system becomes equilibrated and the gas molecules are diffused. Gas moelcules are diffuse and adsorbed by driving force along the x−axis.

Table 2. Parameters Related to the Adsorbates (CO_2 and N_2)[35].

Molecules	Atoms	Charge	σ(Å)	ε/k_B(K)
N_2	N	−0.482	3.31	36.0
	N−*COM*	+0.964		0.0
CO_2	C	+0.70	2.80	27.0
	O	−0.35	3.05	79.0

Gas Adsorption Experiment

Gas adsorption experiments were performed on isolated kerogen from the bulk shale based on already established procedures[36]. Briefly, we collected the samples and removed the bitumen using a mixture of methanol and toluene. Then, we added HCl into the solid residue to remove carbonates. Subsequently, HF was added to remove the silicate minerals and finally pyrite was removed by using $CrCl_2$ and finally, acid with dissolved iorganic minerals were separated from the organic matter by centrifugation.

After isolation from the rock matrix, the solid kerogen was degassed for at least 8 hours at 110 °C to remove moisture and volatiles, crushed (to less than 250 um size) and loaded into the instruments. Low−pressure N_2 was measured on a Micromeritics® Tristar II apparatus at 77 K while CO_2 adsorption was performed on a Micromeritics® Tristar II plus apparatus at 273 K. The gas adsorption quantity was measured over the relative equilibrium adsorption pressure (P/P_0) range of 0.01−0.99, where P is the gas vapor pressure in the system and P_0 is the saturation pressure of N_2.

Results and Discussion

Bakken Molecular Models

The Bakken Shale models were constructed and verified by analyzing experimental data coupled with computational techniques (molecular builder, quantum mechanics calculations, and Monte Carlo/molecular dynamics simulation). The models consist of a complicated mixture of chain and mesh structures. Figure 2 visualizes the three molecular models, before and after optimization

process, which do not have the same chemical composition and structure. The final chemical compositions of Model A, B, and C are $C_{141}H_{187}N_6O_{15}S_4$, $C_{152}H_{193}N_6O_{15}S_4$, and $C_{158}H_{207}N_6O_{16}S_4$, respectively.

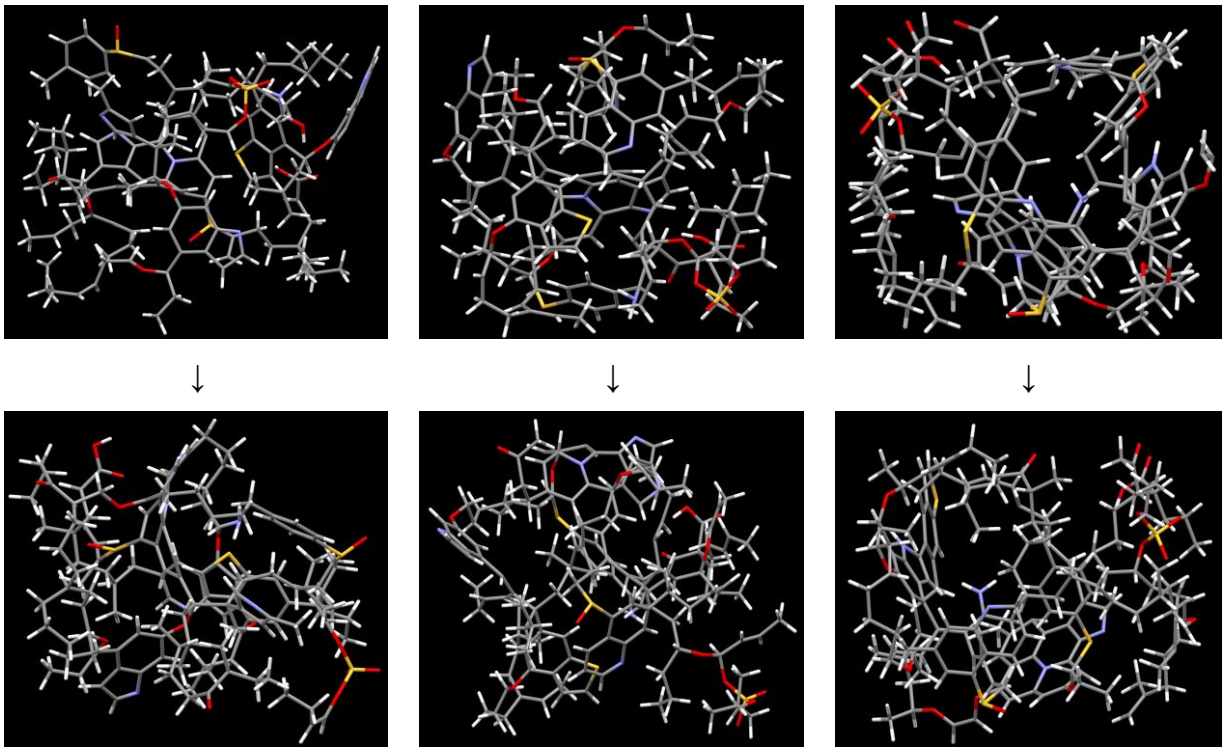

(a) (b) (c)

Figure 2. Constructed and optimized Bakken kerogen model A (a), model B (b), and model C (c). Different geometric configuration and chemical compositions with the following color code, carbon: black; hydrogen: white; oxygen: red; sulfur: yellow and nitrogen: blue. (a) $C_{141}H_{187}N_6O_{15}S_4$, (b) $C_{152}H_{193}N_6O_{15}S_4$, and (c) $C_{158}H_{207}N_6O_{16}S_4$.

Table 3. Structural Parameters Relevant to Carbons in the Bakken Kerogen (sample B1[20]) and the constructed models, Models A, B, and C.

Structure	Sample B1	Model A	Model B	Model C
Aromatic	0.35	0.371	0.344	0.330
Carboxyl/Amide/Carbonyl	0.02	0.028	0.026	0.025
Protonated aromatic	0.17	0.180	0.180	0.140
Phenoxy/Phenolic	0.02	0.021	0.021	0.021
Alkyl-substituted aromatic	0.08	0.064	0.064	0.070
Bridged aromatic	0.09	0.092	0.092	0.092
Aliphatic	0.63	0.61	0.63	0.64
Methylene/Methine	0.46	0.44	0.45	0.48
Methyl/Methoxy	0.15	0.12	0.12	0.13
Alcohol/Ether	0.06	0.04	0.04	0.04
H/C ratio	1.22	1.32	1.27	1.31
Average Density (g/cm^3)	-	0.927	0.919	0.974

Note: the data presented here are ratio per 1 number of carbon.

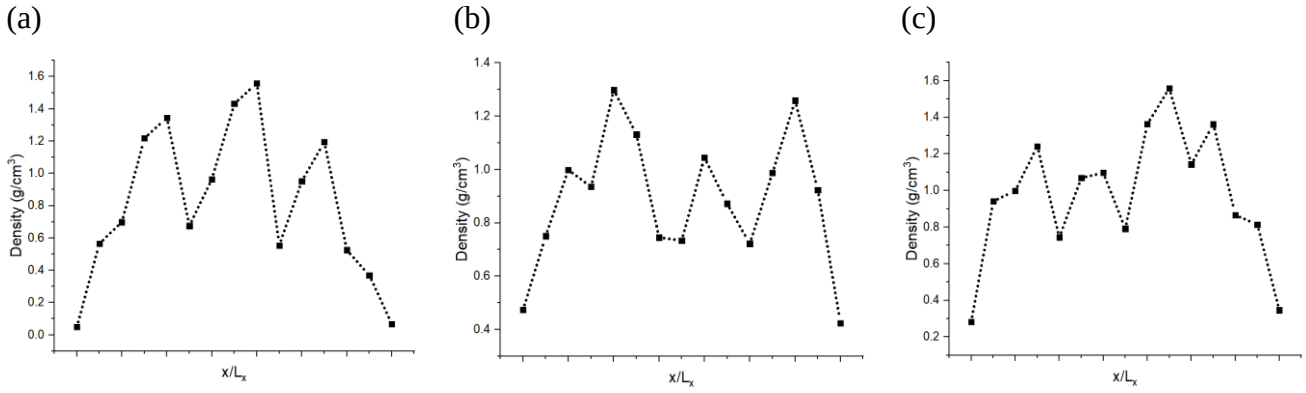

Figure 3. Density(g/cm^3) profiles of the model A (a), B (b), and C (c) along the x−axis.

Table 3 summarizes the aromatic carbons in the constructed models that were found compatible with ^{13}C−NMR data in sample B1. Since aromatic carbons were set up at the initial stage of molecular model building, where aromatic fragments were prebuilt, carbons in aromatic structures are very close to sample B1 in regard to the structural parameters (e.g. protonated, non−protonated, and bridged carbon in aromatic structure). However, some discrepancies were detected such as the

ratio of hydrogen to carbon atoms and methylene/methine structure. Because we improved the models by adding or removing methyl groups and hydrogens, it was not possible for every structure parameter of the models to meet the sample B1 perfectly.

The models have the average densities between 0.92 and 0.98 g/cm^3 (in table 3) demonstrating density profiles along the x−axis around 1.6 to 0.1 g/cm^3 (in Figure 3). The density profiles of models exhibits that the generated kerogen stuructures are amorphous and its internal/external surfaces are rough at the sub-nanometer level in Figure 3. Since gas moelcules diffuse and adsorped along the x—axis (Figure 1), the gas molecules could heavily be affected this internal density of kerogen models.

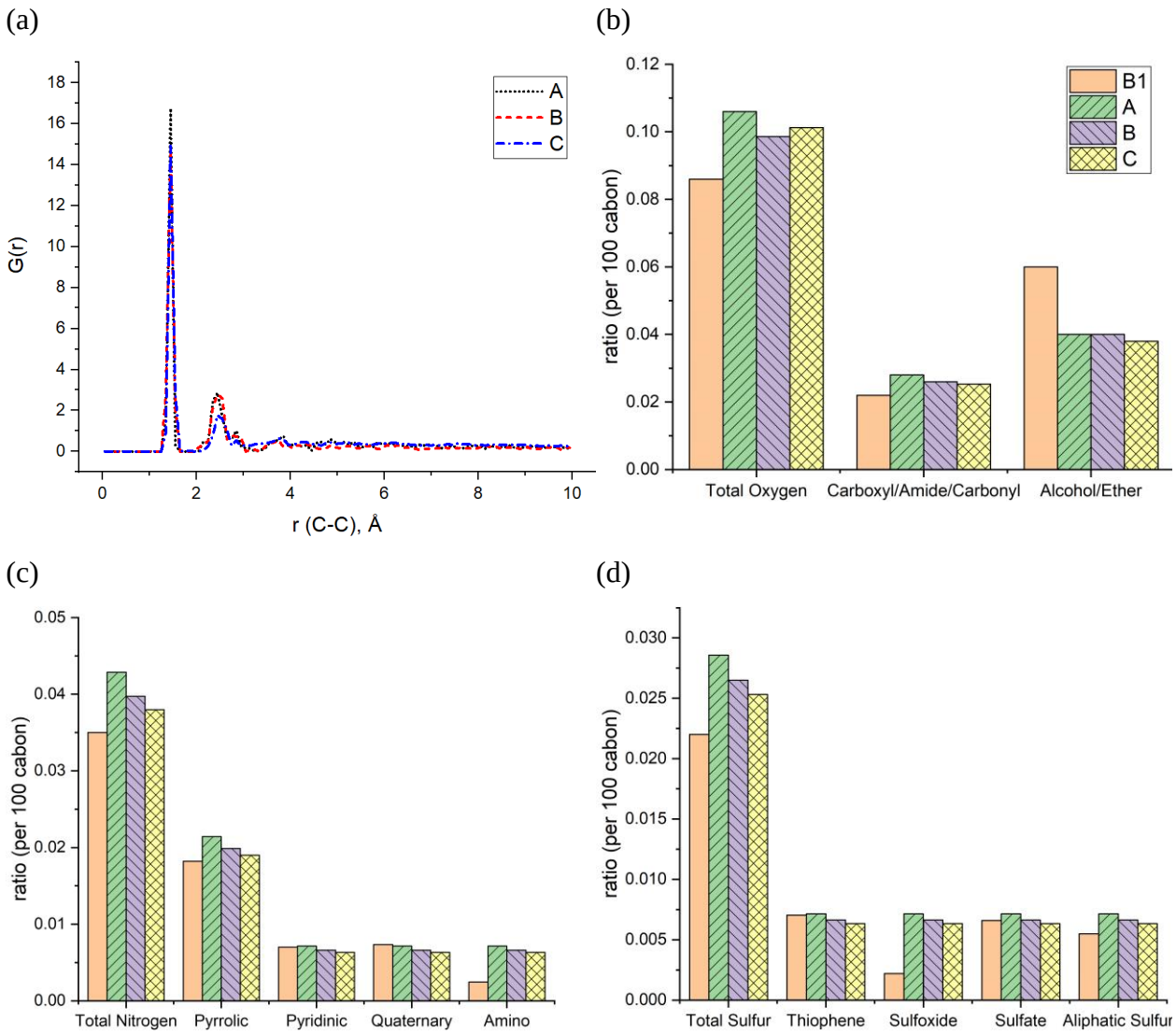

Figure 4. (a) Pair distribution functions (PDF) or G(r) of the Bakken kerogen models. The comparison between sample B1 and the models in terms of (b) the ratio of oxygen-containing functional groups, (c) the ratio of nitrogen-containing functional groups, and (d) the ratio of sulfur-containing functional groups.

The pair distribution function (PDF) profile, Figure 4a, shows the probability of carbon existence at the distance r (Å) from another carbon, and it is exclusively related to carbon structure. The highest peak position is between 1.4 and 1.45 Å which represents aromatic carbons. Since almost 35% of the carbons in the models have an aromatic structure, this is the highest peak of all. The three models have similar peak positions with a similar width. Figure 4b shows the comparison of the three models with sample B1 based on the total oxygen, *i.e.* carbonyl, ether and alcohol groups per 100 carbons. It is apparent from this Figure that the constructed models (Model A−C) contain a higher total number of oxygens per carbon than sample B1. It is the result of sample B1 having a higher number of ether and alcohol groups compared to the models but a similar ratio of carbonyl functional groups. Figures 4c and 4d also indicate that both prebuilt aromatic fragments (pyrrolic, pyridinic, and thiophene) and the bridges (quaternary, sulfate, and aliphatic sulfur) have comparable ratio with sample B1. However, the ratio of amino and sulfoxide in the models are somewhat higher. Screening Figures 4b-d, one can also find that all three models have a smaller percentage of oxygen, nitrogen, and sulfur atoms than the original input data from XPS of sample B1. Our macromolecule models of Bakken kerogen consist of around 150 carbon atoms due to the size limitation of the model building. This limited total number of atoms in the models is not enough to thoroughly represent the perfect ratios.

Gas Diffusion/Adsorption on the Surface of Kerogen

The ultimate goal of this study is to develop reliable amorphous kerogen molecular models. In order to verify the reliability of these models, here we compare and contrast the gas adsorption/diffusion simulation results of these models with the experimental gas adsorption isotherms that we have obtained from Bakken kerogen samples B2 and B3. We performed GCMC/MD simulations to investigate N_2 and CO_2 gas molecular adsorption on the surface of the models as well as their diffusion to the sub-surface levels. Apart from validating our models,

because the three kerogen models cover a variety of structure and chemical composition and contain small size pore ($< 1\ nm$) that are irregularly spread all over the models, we expect that this study sufficiently clarifies the behavior of N_2 and CO_2 molecules through the small size pores of organic matter.

First, we focus on the results of adsorption/diffusion of N_2 molecules on/into three molecular Models A-C and compare the results to the experimental N_2 adsorption isotherms of samples B2 and B3 in Figure 5.

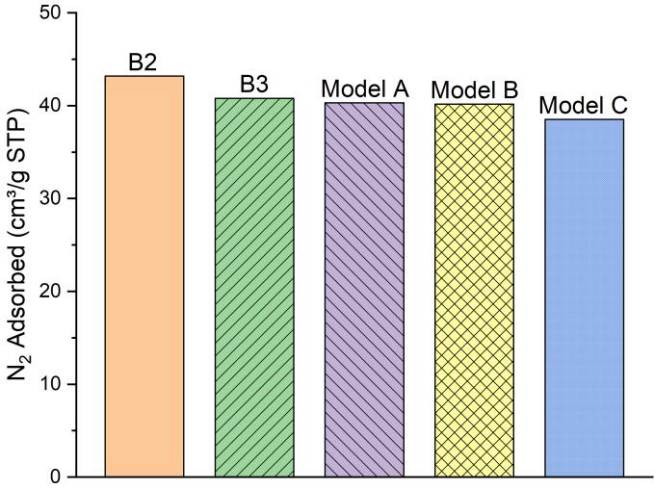

Figure 5. The comparison of the simulated excess nitrogen (N_2) adsorption isotherms between the models (Model A−C) with experimental loadings (sample B2 and B3) at 100 kPa, 77 K.

As can be clearly seen, samples B2 and B3 capture around 43.18 and 40.78 (cm^3/g STP) of the N_2 gas, respectively, at 100 kPa and 77 K. N_2 molecules adsorption behavior with the Models A and B (40.29 and 40.15 cm^3/g STP, respectively) are fairly close to the two experimental samples. Meanwhile, the number of adsorbed molecules into Model C (38.5 cm^3/g STP) is almost 4 % lower than both of the other two Models and the experimental samples B2 and B3. We conclude that the difference of functional group distribution and internal density profile among the three models affects the adsorption of N_2 molecules on the kerogen surface and pores. For instance, Model C containing a larger ratio of aliphatic carbon structure, especifically more methyl groups, cannot provide adequate space for N_2 molecules for adsorption as much as Models A and B. The steric

effect of the methyl groups may be the main reason preventing the attachement of N_2 molecules to the framework compared to the planar configurations of aromatic structures[37].

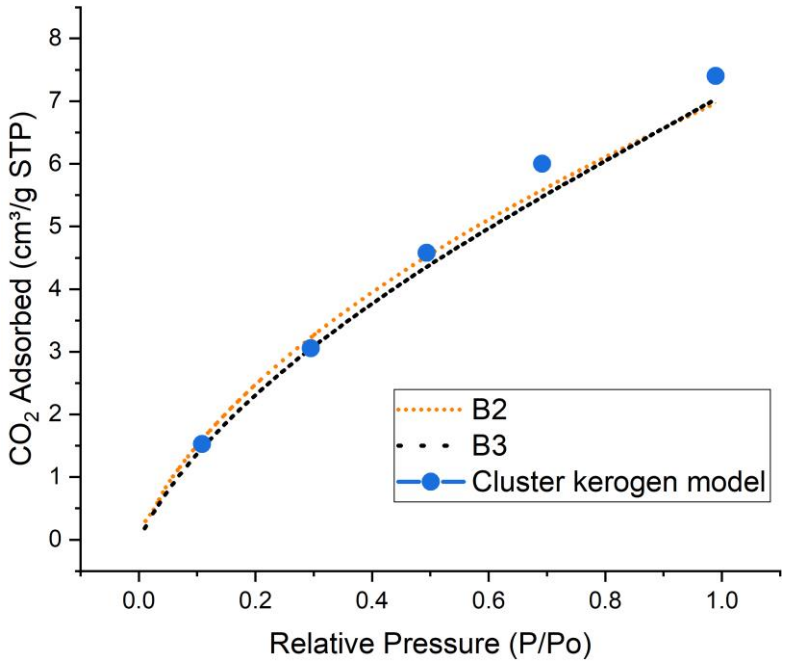

Figure 6. Comparison of simulated excess CO_2 adsorption isotherms between the cluster kerogen Model, blue dots, and the experimental samples B2, orange, and B3, black, at 273K.

Since, the overall results of N_2 adsorption on the three models were close to the experiment, we clustered the three models for CO_2 gas adsorption and diffusion simulations. Packmol package was utilized to place one of each kerogen models (Models A, B, and C) in two sides of a feed compartment with the size of around 16 x 57 x 40 angstrom, as shown in Figure 1. These two systems were then allowed to come to relaxation by running a 1 ps NVT molecular dynamics simulations. The final average density of kerogen models compartment is 0.922 g/cm^3. Since the three kerogen models were simply adhered to one another and clustered, packing them in different modes was not considered. In this system, gaseous fluids would diffuse to two different surfaces of the clustered kerogen model. Unlike N_2 gas adsorption experimental conditions, CO_2 gas adsorption experiment, and accordingly theoretical simulations, were performed under a series of varying pressure values at 273 K (Figure 6).

The result of CO_2 gas adsorption isotherms of the samples B2 and B3 show a nearly linear relationship of gas adsorption with respect to the pressure. The cluster Model very closely follows this behavior and only slightly deviates at higher pressure. At lower pressure of 10, 30, and 50 kPa, the cluster Model shows a total amount of adsorbed CO_2 molecules of 1.53, 3.05, and 4.58 cm^3/g STP, respectively. These are very close to those of experimental samples B2 (1.59, 3.22, and 4.52 cm^3/g STP), and B3 (1.45, 3.05, and 4.35 cm^3/g STP). The small discrepancy, around 5%, between the cluster model and samples B2 and B3 occurs when the simulation and experimental pressures reach 70 kPa. This phenomenon can be explained due to the increase in chemical potential in the smaller pores (ultra−micro pore, $<70^{-1}nm$). Its reported that the potential between gas molecules and pore surfaces is overlapped and leads to higher amounts of CO_2 molecules to be adsorbed in smaller pores compared to the larger ones[38,39]. Since the models host ultra−micro pores ($30^{-1}nm$ to $70^{-1}nm$) and a greater number of CO_2 molecules are placed in a fixed system at higher pressures (larger number of CO_2 molecules in GCMC/MD simulation), it's expected that larger quantities of CO_2 be adsorbed on the pore surfaces, which is in contrast with samples B2 and B3 that both contain meso (less than $3-5\ nm$) and ultra−micro pores. The results proclaim that the pore structure plays an important role in adsorption mechanisms as a function of pressure.

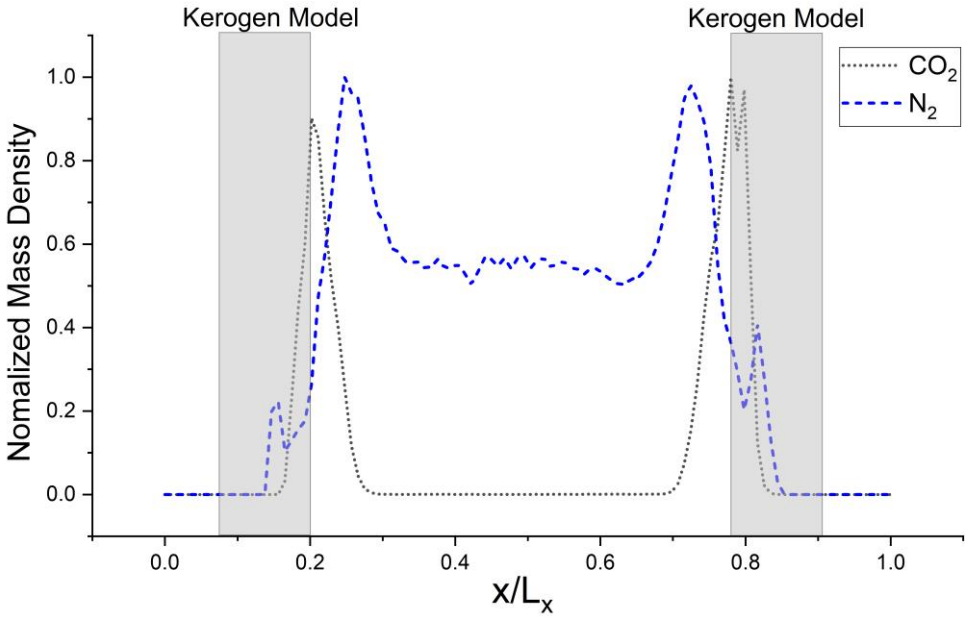

Figure 7. Normalized mass density profile of CO_2 from clustered Bakken kerogen models at 100 kPa and 273 K, and of N_2 from kerogen model A at 100 kPa and 77 K from GCMC/MD simulation.

This density profile shows that CO_2 and N_2 molecules are crowded near Bakken models at one million timesteps.

The simulated mass density profile in Figure 7 shows that CO_2 and N_2 molecules have migrated to the kerogen model during the process and penetrated to the sub-surface levels of the model as well as being adsorbed on the surface. This simulation confirms that the interaction between gas (CO_2 and N_2) molecules and kerogen molecular Models is strong enough to capture the molecules on or inside the Models. Because the internal density of model is irregular and highly densed sub-surfaces are existed (Figure 3), the gas molecules could be captured into these densed areas inside kerogen model. In particular, CO_2 molecules show a much stronger interaction than N_2 such that a considerable number of CO_2 molecules penetrate to the sub-surface levels of the kerogen Model. N_2 molecules, on the other hand, are mostly diffused in the bulk region with a smaller number of molecules detained on the surface of the kerogen Model. These results demonstrate that kerogen can be used as a porous filter for optimal separation of CO_2 and N_2 gas molecules.

Conclusion

In this work we reported a molecular model for amorphous organic matter (kerogen) built based on experimental constraints. The numerical analysis of the kerogen by the methods ^{13}C−NMR, XPS, and XANES was used to determine the chemical composition and structure of three different Models. GAFF parameters combined with partial charges computed via quantum mechanics calculations were used to build a more realistic Model. GCMC and MD simulations were run to compute N_2 and CO_2 gas adsorption isotherms on the Model and were compared to our experimental results. N_2 gas adsorption behavior in the three kerogen Model systems was in very good agreement with experimental results in similar conditions, 100 kPa and 77 K. Adsorption of CO_2 molecules on a clustered Model also shows similar adsorption isotherm behavior overall. Based on the simulation results we uncovered, the kerogen Model seems to have a stronger interaction with CO_2 molecules than N_2 molecules such that CO_2 molecules are not only adsorbed on the surface but also penetrate to the sub-surface level of the Model.

References

1 B. Jia, J.-S. Tsau and R. Barati, *Fuel*, 2019, **236**, 404–427.

2 Y. Shen, H. Ge, C. Li, X. Yang, K. Ren, Z. Yang and S. Su, *J. Nat. Gas Sci. Eng.*, 2016, **35**, 1121–1128.

3 E. Fathi and I. Y. Akkutlu, *Int. J. Coal Geol.*, 2014, **123**, 52–61.

4 A. Vengosh, R. B. Jackson, N. Warner, T. H. Darrah and A. Kondash, *Environ. Sci. & Technol.*, 2014, **48**, 8334–8348.

5 A. Muggeridge, A. Cockin, K. Webb, H. Frampton, I. Collins, T. Moulds and P. Salino, *Philos. Trans. A. Math. Phys. Eng. Sci.*, 2013, **372**, 20120320.

6 C. Guo, M. Wei and H. Liu, *PLoS One*, 2018, **13**, e0188480.

7 B. Durand, *Sedimentary Organic Matter and Kerogen. Definition and Quantitative Importance of Kerogen. Kerogen, Insoluble Organic Matter from Sedimentary Rock*, Editions technips, 1980.

8 H. Wang, Z. Qu, Y. Yin, J. Bai and B. Yu, *J. Therm. Sci.*, 2019, **28**, 1–16.

9 M. Vandenbroucke and C. Largeau, *Org. Geochem.*, 2006, **38**, 719–833.

10 A. Abarghani, M. Ostadhassan, T. Gentzis, H. Carvajal-Ortiz and B. Bubach, *Int. J. Coal Geol.*, 2018, **188**, 79–93.

11 C. Bousige, C. M. Ghimbeu, C. Vix-Guterl, A. E. Pomerantz, A. Suleimenova, G. Vaughan, G. Garbarino, M. Feygenson, C. Wildgruber, F.-J. Ulm, R. J.-M. Pellenq and B. Coasne, *Nat. Mater.*, 2016, **15**, 576–582.

12 A. L. Burlingame, P. A. Haug, H. K. Schnoes and B. R. Simoneit, *Adv. Org. Geochemistry 1968*, 1969, 85–129.

13 R. E. P. M. Siskin, C. G. Scouten, K. D. Rose, T. Aczel, S. G. Colgrove, *Detailed Structural Characterization of the Organic Material in Rundle Ramsay Crossing and Green River Oil Shales*, Composition, Geochemistry and Conversion of Oil Shales, 1995,

vol. 455.

14 P. Ungerer, J. Collell and M. Yiannourakou, *Energy & Fuels*, 2014, **29**, 91–105.

15 J. J. P. Stewart, *J. Mol. Model.*, 2013, **19**, 1–32.

16 H. Lee, F. A. Shakib, M. Shokouhimehr, B. Bubach, L. Kong and M. Ostadhassan, *J. Phys. Chem. C*, 2019, **123**, 20877–20883.

17 J. Collell, P. Ungerer, G. Galliero, M. Yiannourakou, F. Montel and M. Pujol, *Energy & Fuels*, 2014, **28**, 7457–7466.

18 S. Tesson and A. Firoozabadi, *J. Phys. Chem. C*, 2018, **122**, 23528–23542.

19 G. Liu, J. A. Sorensen, J. R. Braunberger, R. Klenner, J. Ge, C. D. Gorecki, E. N. Steadman and J. A. Harju, *SPE Unconv. Resour. Conf.*, 2014, 7.

20 S. R. Kelemen, M. Afeworki, M. L. Gorbaty, M. Sansone, P. J. Kwiatek, C. C. Walters, H. Freund, M. Siskin, A. E. Bence, D. J. Curry, M. Solum, R. J. Pugmire, M. Vandenbroucke, M. Leblond and F. Behar, *Energy & Fuels*, 2007, **21**, 1548–1561.

21 J. Tong, X. Han, S. Wang and X. Jiang, *Energy & Fuels*, 2011, **25**, 4006–4013.

22 F. Behar, V. Beaumont and H. L. De B. Penteado, *Oil Gas Sci. Technol. - Rev. IFP*, 2001, **56**, 111–134.

23 M. D. Hanwell, D. E. Curtis, D. C. Lonie, T. Vandermeersch, E. Zurek and G. R. Hutchison, *J. Cheminform.*, 2012, **4**, 17.

24 J. Wang, W. Wang, P. A. Kollman and D. A. Case, *J. Mol. Graph. Model.*, 2006, **25**, 247–260.

25 J. Wang, R. Wolf, J. Caldwell, P. Kollman and D. Case, *J. Comput. Chem.*, 2004, **25**, 1157–1174.

26 J. Gasteiger and M. Marsili, *Tetrahedron Lett.*, 1978, **19**, 3181–3184.

27 S. Plimpton, *J. Comput. Phys.*, 1995, **117**, 1–19.

28 L. Martínez, R. Andrade, E. Birgin and J. M. Martínez, *J. Comput. Chem.*, 2009, **30**,

2157–2164.

29 T. Hočevar and J. Demčar, *J. Stat. Softw.*, , DOI:10.18637/jss.v071.i10.

30 J. Tirado-Rives and W. L. Jorgensen, *J. Chem. Theory Comput.*, 2008, **4**, 297–306.

31 F. L. Hirshfeld, *Theor. Chim. Acta*, 1977, **44**, 129–138.

32 W. Humphrey, A. Dalke and K. Schulten, *J. Mol. Graph.*, 1996, **14**, 33–38.

33 W. M. Brown, A. Kohlmeyer, S. J. Plimpton and A. N. Tharrington, *Comput. Phys. Commun.*, 2012, **183**, 449–459.

34 S. Plimpton, R. Pollock and M. Stevens, *Proc. 8th SIAM Conf. Parallel Process. Sci. Comput.*

35 J. Potoff and J. Siepmann, *AIChE J.*, 2001, **47**, 1676–1682.

36 K. Liu, M. Ostadhassan, J. Zou, T. Gentizs and R. Rezaee, *Fuel*, 2017, **209**, 567–578.

37 R. G. Kadesch and S. W. Weller, *J. Am. Chem. Soc.*, 1941, **63**, 1310–1314.

38 P. Psarras, R. Holmes, V. Vishal and J. Wilcox, *Acc. Chem. Res.*, 2017, **50**, 1818–1828.

39 Y. Liu and J. Wilcox, *Environ. Sci. Technol.*, 2012, **46**, 1940–1947.